Original Article

Modelling plant canopy effects on water-heat exchange in the freezing-thawing processes of active layer on the Qinghai-Tibet Plateau

GUO Lin-mao[1,2] https://orcid.org/0000-0002-4892-8735; e-mail: guolm17@lzu.edu.cn

CHANG Juan[1*] https://orcid.org/0000-0001-7268-5000; ✉e-mail: changjuan@lzu.edu.cn

XU Hong-liang[1] https://orcid.org/0000-0002-5559-5916; e-mail: xuhl18@lzu.edu.cn

SUN Wen-jun[1] https://orcid.org/0000-0002-8046-3712; e-mail: sunwj2019@lzu.edu.cn

*Corresponding author

1 *Key Laboratory of Western China's Environmental Systems (Ministry of Education), College of Earth and Environmental Sciences, Lanzhou University, Lanzhou 730000, China*

2 *State Key Laboratory of Hydraulics and Mountain River Engineering, College of Water Resource and Hydropower, Sichuan University, Chengdu, 610000, China*

Abstract: The effect of vegetation on the water-heat exchange in the freezing-thawing processes of active layer is one of the key issues in the study of land surface processes and in predicting the response of alpine ecosystems to climate change in permafrost regions. In this study, we used the simultaneous heat and water model to investigate the effects of plant canopy on surface and subsurface hydrothermal dynamics in the Fenghuoshan area of the Qinghai-Tibet Plateau by changing the leaf area index (LAI) and keeping other variables constant. Results showed that the sensible heat, latent heat and net radiation are increased with an increase in the LAI. However, the ground heat flux decreased with an increasing LAI. The annual total evapotranspiration and vegetation transpiration ranged from -16% to 9% and -100% to 15%, respectively, in response to extremes of doubled and zero LAI, respectively. There was a negative feedback between vegetation and the volumetric unfrozen water content at 0.2 m through changing evapotranspiration. The simulation results of soil temperature and moisture suggest that better vegetation conditions are conducive to maintaining the thermal stability of the underlying permafrost, and the advanced initial thawing time and increasing thawing rate of soil ice with the increase in the LAI may have a great influence on the timing and magnitude of supra-permafrost groundwater. This study quantifies the impact of vegetation change on surface and subsurface hydrothermal processes and provides a basic understanding for evaluating the impact of vegetation degradation on the water-heat exchange in permafrost regions under climate change.

Keyword: Permafrost; Simultaneous heat and water model; Leaf area index; Water-Heat exchange; Thermal-moisture dynamics

Notations

Acronym	Description
LAI	Leaf area index
R_n	Net radiation
H	Sensible heat
LE	Latent heat
G_0	Ground heat flux
E_{total}	Total evaportranspiration
E_{trans}	Vegetation transpiration

E_{soil}	Soil evaporation
$\theta_{0.2}$	Volumetric unfrozen water content at 0.2 m
T_{soil}	Soil temperature
M_{soil}	Volumetric soil unfrozen water content
RLC	Ratio of LAI changing
T_{a0}	The first day when the soil temperature was greater than 0 °C for 7 consecutive days
T_{b0}	The first day when the soil temperature was less than 0 °C for 7 consecutive days
$\triangle T_{max}$	The difference between summer ground temperature peak value and initial thawing temperature (0 °C)
$\triangle T_{min}$	The difference between the initial freezing temperature (0 °C) and the minimum ground temperature at completely frozen period

1 Introduction

The water and heat exchange between the land-atmosphere systems in permafrost regions, being affected by the surface characteristics, microtopography, geology, and hydrology (Zhang et al. 2017), have significant impacts on ecosystem processes, hydrologic cycles, and climate change (Chang et al. 2019; You et al. 2017). The thermal-moisture dynamics of the active layer are the main factors that control water cycles and surface energy balance (Wang et al. 2009), which directly affect the ecological environment, hydrological processes and stability of permafrost in cold regions (Li et al. 2019; Wen et al. 2014). Several studies have shown that surface characteristics, such as snow cover and soil conditions, especially vegetation, significantly influence the thermal-moisture coupling cycles in permafrost regions (Chang et al. 2014; Wang et al. 2009; Wang et al. 2012; Yi et al. 2009). Wang et al. (2012) reported that different vegetation types and cover will lead to differences in the convective transport efficiencies of surface water and heat, thereby affecting the freezing-thawing cycles in the active layer and the thermal condition of the permafrost. Shur and Jorgenson (2007) reported that vegetation cover protects or drives permafrost changes by changing the water-thermal coupling cycles. The degradation of vegetation in permafrost regions not only leads to a loss of fine soil particles, reduction in soil organic matter, and deterioration of water sorption and thermal conductivity (Wang et al. 2009; Wang et al. 2012), but also affects the regional climate by imposing changes in surface water-heat exchange (Chen et al. 2009; You et al. 2017) and regional ecology, resulting in a profound impact on the entire biosphere (Christensen et al. 2004; Jorgenson et al. 2001). The relationship between the surface and subsurface hydrothermal processes (of the active layer) and vegetation, especially the effects of different vegetation cover on hydrothermal processes, has become a significant indicator of climate change (Guglielmin et al. 2008). However, the effect of vegetation changes affects the thermal-moisture dynamics and surface water-heat exchange process, along with the extent of this impact, are still unclear.

The Qinghai-Tibet Plateau (QTP) is the largest high-altitude permafrost area with an area of approximately 1.06×10^6 km² (Zou et al. 2017). The unique thermodynamic process on the QTP, due to its high elevation (over 4000 m on average) and distinct location in mid-low latitude, has a great influence on the Asian monsoon and global climate change, further affecting the global energy and water cycles (Karl and Trenberth 2003). Alpine meadows and alpine swamp meadows are the main vegetation types in the QTP. In the past 15 years (1986–2000), the areas of high vegetation covered (greater than 85%) alpine meadows and alpine swamp meadows decreased by 5.15% and 24.36% respectively in the source areas of the Yangtze and Yellow Rivers under climate change, indicating serious ecosystem degradation (Qian et al. 2006). Zhong et al. (2019) reported that in the past decades (1999–2014), the vegetation density generally shows an increasing trend, accounting for more than 80% of the total QTP territory under the joint influence of human activity [such as Natural Forest Conservation Program (Zhang et al. 2000) and the establishment of the State Integrated Test and Demonstration Region of the Three-Rivers Headwater Region (Fang 2013)] and climate change. Variations in energy balance and water cycles caused by the response of the permafrost region's alpine ecosystems to climate change would most likely be reflected in the changes in the moisture and associated heat of the permafrost soil (Wang et al. 2009). Therefore, mechanisms that govern the variations in soil moisture and temperature are important to understand the regional variations in water-heat exchange that arise from global climate change. However, the mechanism and characterization of the effects of vegetation on surface and subsurface

hydrothermal processes of the active layer have not been studied much because of the lack of systematic and comprehensive observations. Therefore, it is urgent to fully understand the response of water cycles and surface energy balance of the alpine ecosystem to vegetation change, and the accompanying changes in the thermal-moisture dynamics of the active layer (Wang et al. 2012; Wang et al. 2007; Zhang et al. 2010). However, the harsh climate and environmental conditions make it difficult to conduct field observations in permafrost regions. Therefore, the geophysical model is considered a useful tool for studying the changes in the thermal-moisture dynamics in permafrost regions (Frampton et al. 2013).

Because of the seasonal freezing-thawing cycle of frozen ground, the model involving the thermal process of soil phase change becomes the first choice to simulate the soil thermal-moisture regime in cold regions. Several models such as the Geophysical Institute Permafrost Laboratory 2 (GIPL2) (O'Donnell et al. 2011; Qin et al. 2017a), Geomorphology-based Ecohydrological Model (GBEHM) (Gao et al. 2018; Wang et al. 2018), CoupModel (Rasmussen et al. 2018; Zhou et al. 2013), Distributed Water-Heat Coupled Model (DWHC) (Chen et al. 2006), TTOP (Yin et al. 2016), and FEFLOW-piFreeze (Langford et al. 2020; Magnin et al. 2017), have been widely used to simulate the soil thermal-moisture dynamics in cold regions. These models either require high input parameters or take less consideration of the surface energy-water exchange process. The simultaneous heat and water model (SHAW), which fully considers the water phase transition and the accompanying water-thermal coupling processes during the soil freezing and thawing processes, has been widely used in the study of thermal-moisture dynamics of the active layer, water-heat exchange between the land-atmosphere systems and changes of land surface ecological environment, which makes up for the disadvantage of inadequate observation data in permafrost regions to a great extent. Guo and Yang (2010) simulated the soil temperature and moisture dynamics and analyzed the effect of surface heat flux on the soil temperature in the seasonal frozen regions of the central QTP using the SHAW model. Zhou et al. (2008) used the SHAW model to reveal the influence of soil freezing-thawing process on the energy-water cycle with respect to surface-vegetation-atmosphere processes in the alpine meadow regions of the QTP.

Langford et al. (2020) calculated the ground temperature and surface water balance in the Scotty Creek drainage basin using the SHAW model. In the SHAW model, leaf area index (LAI), as one of the important vegetation input parameters, is used to calculate the surface energy balance and canopy transpiration. Although, the ground heat flux is the smallest energy partitioning of the surface energy budget, it directly determines the soil temperature profile of the active layer, which in turn affects the soil moisture regime. In addition, the canopy transpiration process still affects the distribution of shallow soil moisture. Therefore, this study used the developed SHAW model to explore the effects of plant canopy on the surface and subsurface hydrothermal processes of the active layer by changing the LAI, while keeping the other variables constant. The objectives of our study are to: (1) compare the differences in the energy partitioning under different ratios of LAI changing (RLC) and examine the effects of plant canopy changes on it; and (2) quantify the variations in the thermal-moisture dynamics of the active layer response to the changes in the LAI.

2 Materials and Methods

2.1 Site description and data collection

The study area is located in the Zuomaoxikong watershed of the FHS (Fenghuoshan area) on the QTP (92°50'-93°03'E, 34°40'−34°48'N, Fig. 1). The Zuomaoxikong watershed is an important branch of the Beiluhe in the source area of the Yangtze River (SAYR), which belongs to a typical continuous permafrost area. The observation of soil temperature (T_{soil}) and moisture (M_{soil}, volumetric soil unfrozen water content) were constructed in a typical alpine meadow area, where permafrost is well developed. The altitude of the study area ranges from 4603 to 5403 m and the annual average temperature is - 5.2°C; the annual average precipitation is 290.9 mm, annual average relative humidity is 57%, and permafrost thickness ranges from 50 to 120 m with the active layer thickness ranging from 0.8 to 2.5 m (Chang et al. 2015). There are no glaciers in the Zuomaoxikong watershed, the main recharge of rivers is precipitation, snow melt water and groundwater. Alpine meadows are the main vegetation types in the study area and the dominant vegetation communities consist of
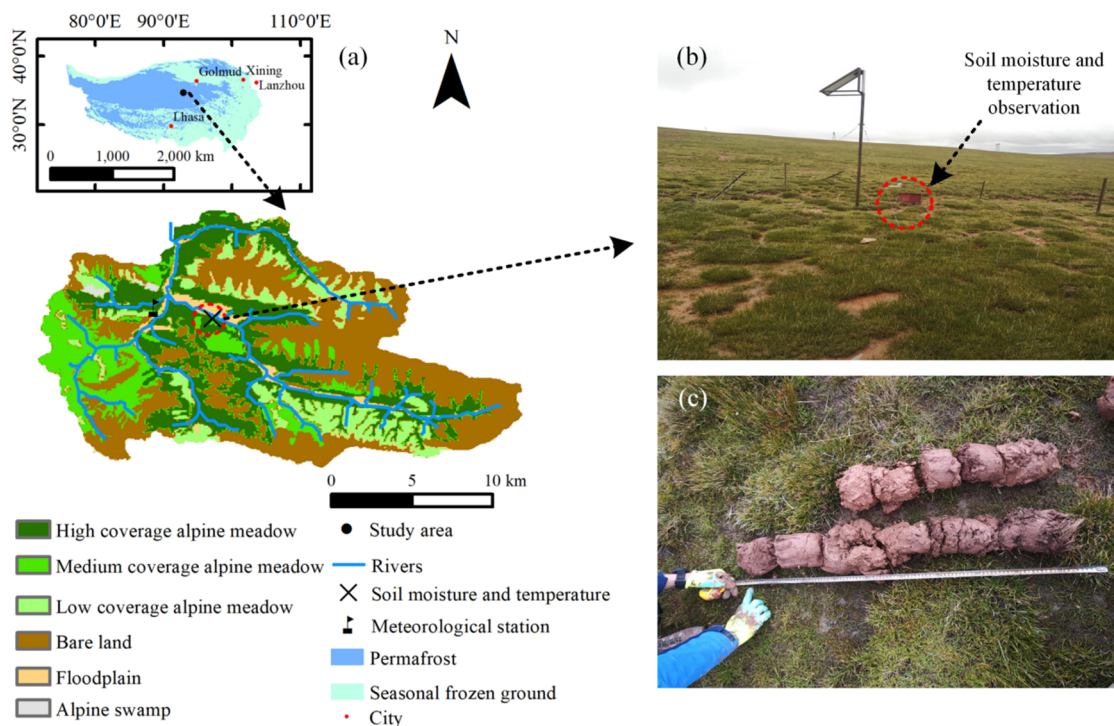
Fig. 1 (a) Location of the study area, (b) site observations setup, (c) soil sample.

Table 1 List of measured items and instruments

Measurements	Instruments	Accuracy	Height/depth (m)
Air temperature (°C)	HMP155, Vaisala	± 0.2°C	2.0
Relative humidity (%)	HMP155, Vaisala	± 2%	2.0
Wind speed (m·s⁻¹)	5106, Young	± 0.3 m·s⁻¹	2.0
Precipitation (mm)	52202, Young	± 1%	0.5
Global radiation (W·m⁻²)	CM3, Campbell	± 10%	2.0
Soil temperature (°C)	5TM, Meter	± 1°C	-0.05, -0.2, -0.5, -1.0, -1.6
Soil moisture (m³·m⁻³)	5TM, Meter	± 0.03 m³·m⁻³	-0.05, -0.2, -0.5, -1.0, -1.6

Kobresia pygmaea, *Kobresia humilis* and *Kobresia capillifolia*. The average height of vegetation is about 20 cm, and the root depth is concentrated at 0–30 cm which can reach a depth of maximum 100 cm (Zhang et al. 2012). The growing and non-growing seasons are May to September and October to April, respectively (Wang et al. 2012), and the monsoon usually starts at the beginning of May and ends at the end of September (Gu et al. 2015).

A portable micro-meteorological station (HOBO Weather Station, ONSET Co., USA) was established 2.0 m above the experimental field to record the air temperature, precipitation, relative humidity, global radiation, air pressure and wind speed every half hour. A 1.6 m deep borehole was drilled, and soil moisture and temperature sensors were installed at depths of 0.05, 0.20, 0.50, 1.0 and 1.60 m. The recording period of the above-mentioned observation items was from January 1, 2017, to October 31, 2019. The related

information of the observation instruments for each item is shown in Table 1.

2.2 Model description

The SHAW model was developed by Flerchinger and Saxton (1989) to simulate the transport and exchange of water, heat and solute fluxes in one-dimensional profiles during soil freezing and thawing which includes the effects of plant cover, dead plant residue, and snow. This model has a clear mathematical description of the physical processes of the material and energy exchange between different layers of the system. The simultaneous calculation of heat, water and solute fluxes provides an accurate simulation of the dynamic changes of the soil temperature and moisture, water flux between soil nodes, evapotranspiration, surface energy budget, and ground surface temperature in the freezing-thawing processes.

Table 2 Soil particle size distribution in the Fenghuoshan observation point

Depth (cm)	Soil particle content (%)						
	1-2 mm	0.5-1 mm	0.25-0.5mm	0.05-0.25 mm	0.02-0.05 mm	0.002-0.02 mm	<0.002 mm
0-20	0.001	0.841	2.492	31.562	21.379	35.659	8.066
20-40	0.023	0.501	1.372	26.457	22.649	39.105	9.893
40-70	0.045	1.088	1.418	23.394	21.597	41.563	10.895
70-100	0.004	0.746	1.973	26.308	22.213	39.335	9.421

Table 3 Plant growth parameters used in simultaneous heat and water model (SHAW) model

Stage	Plant height (m)	Dimension (cm)	Dry biomass (kg·m^{-3})	Root depth (m)	Leaf area index
Frozen stage	0.03	0.5	0.10	0.08	0.6
Early growth stage	0.04	0.7	0.20	0.10	1.3
Growth stage	0.08	1.0	0.35	0.15	2.7
Later growth stage	0.06	0.6	0.27	0.13	1.9

Notes: Frozen stage, October to February; Early growth stage, March to May; Growth stage, June to July; Later growth stage, August to September (Zhou et al. 2008)

The input data of the model used in this study mainly includes the initial T_{soil} and M_{soil} profiles; meteorological data (air temperature, precipitation, relative humidity, global radiation and wind speed; Fig. 2), site characteristics information and parameters describing the soil (Table 2), plant, and snow (initial thickness and density). Site characteristics information includes slope, aspect, latitude, and surface roughness. Plant growth parameters will be introduced in detail in Section 2.3. The output of the SHAW model used in this study includes daily soil temperature and moisture (volumetric soil unfrozen water content and ice content), net radiation, latent heat flux, sensible heat flux, ground heat flux, evapotranspiration, transpiration, and soil evaporation. Among them, the ground heat flux was calculated using the surface energy balance equation, and the soil evaporation was obtained by subtracting transpiration from evapotranspiration.

2.3 Model simulation

In this study, the dynamic changes of the T_{soil} and M_{soil} at different depths of the active layer were simulated ranged from January 1, 2017 to October 31, 2019. The simulated soil profile was divided into six layers from 0 m to 1.6 m below the ground (0, 0.05, 0.2, 0.5, 1.0, and 1.6 m). The lower boundary condition of water flow was set as specified soil water content, and the specified temperature was set as the lower boundary condition of temperature. The soil particle size distribution of each layer was measured (Table 2), and the albedo of dry soil and plant were given as 0.3 and 0.2, respectively. Table 3 summarizes
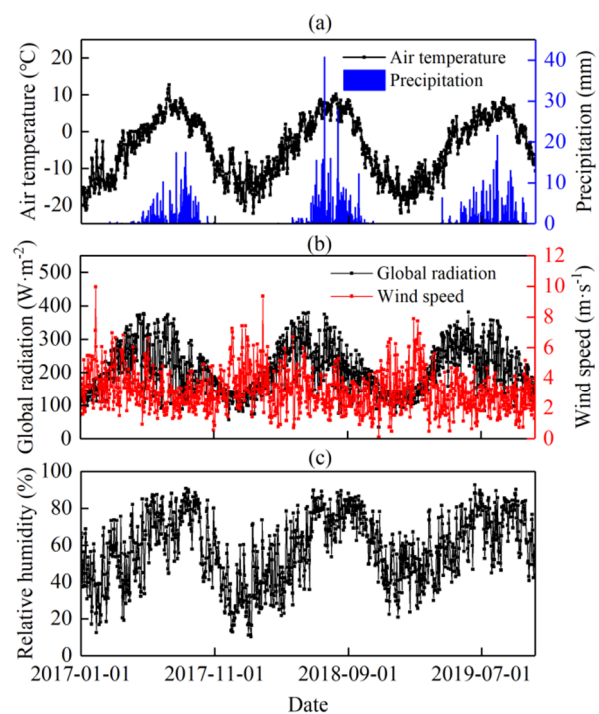

Fig. 2 Input forcing data of the simultaneous heat and water model (SHAW).

the plant growth parameters used in the SHAW model, including plant height (m), characteristic dimension of leaves (cm), dry biomass (kg·m^{-2}), effective root depth (m) (obtained by field measurement), and leaf area index (dimensionless, obtained by scanning the leaf area of grass sample per unit area using LAI 300). The stomatal resistance of plant (r_{so}) was given as 100 s·m^{-1}, and the resistance of the leaves (r_l) and roots (r_r) were given as 1×10^5 and 2×10^5 m^3·s·kg^{-1}, respectively (Zhang et al. 2011); the value of the critical leaf water potential (ψ_c) was given as -300 m.

To investigate the effects of plant canopy on the

Table 4 Model performance measures for soil temperature

Depth (m)	Calibration period (2017/1/1-12/31)			Validation period (2018/1/1-2019/10/31)		
	RMSE (°C)	ME (°C)	NSE	RMSE (°C)	ME (°C)	NSE
0.05	1.758	0.166	0.934	1.951	0.345	0.930
0.20	1.626	-0.035	0.921	1.812	0.095	0.918
0.50	1.371	-0.221	0.893	1.586	-0.053	0.889
1.00	0.844	-0.313	0.889	1.089	-0.124	0.867
1.60	0.033	0.001	0.999	0.037	-0.001	0.999

Notes: RMSE, ME, and NSE denote root mean square error, mean error, and Nash–Sutcliffe efficiency coefficient, respectively.

surface water-heat exchange and thermal-moisture dynamics in the freezing-thawing processes of the active layer, we conducted a sensitivity analysis by changing the LAI and keeping the other model variables constant. The RLC ranged from -100% to +100% corresponding to two extreme scenarios: degradation to bare soil and significant improvement in vegetation, respectively, since vegetation degradation and improvement were all observed in the QTP during the past decade (Han et al. 2019; Zhong et al. 2019). It should be noted that, due to the lack of observed surface energy and evapotranspiration data, this part of the simulation is only to explore its response to the change in the plant canopy, rather than accurate reproduction.

Our study used the period of 2017 for model calibration and the period from January 2018 to October 2019 for model validation. The performance of the developed model can be evaluated using statistical parameters, including the root mean square error (RMSE), mean error (ME), and Nash–Sutcliffe efficiency coefficient (NSE). The formulas for calculating these parameters are as follows:

$$\text{RMSE} = \sqrt{\frac{1}{n}\sum_{i=1}^{n}(S_i - M_i)^2} \tag{1}$$

$$\text{ME} = \frac{1}{n}\sum_{i=1}^{n}(S_i - M_i) \tag{2}$$

$$\text{NSE} = 1 - \frac{\sum_{i=1}^{n}(S_i - M_i)^2}{\sum_{i=1}^{n}(M_i - \bar{M})^2} \tag{3}$$

where n denotes the number of samples, S_i and M_i denote the simulated and measured values, respectively, and $\bar{S}$ and $\bar{M}$ denote the average simulated and measured values, respectively. The best fit b etween the measured and simulated values would have RMSE = 0, ME = 0, and NSE = 1.

3 Model Validation

3.1 Soil temperature

An accurate calculation of the T_{soil} is essential for the simulation of the water-heat exchange between the land-atmosphere systems. A reasonable description of soil heat transfer is a necessary condition for the accurate simulation of the surface energy budget (Zhao et al. 2008). The results show that the simulated T_{soil} at different depths agreed reasonably well with the measured values. The developed SHAW model could exactly identify the varying processes of the T_{soil} within the active layer (Fig. 3). Table 4 summarizes the model performance measures for the T_{soil} at different depths. The RMSE decreased from 1.951°C at 0.05 m to 0.037°C at 1.6 m, indicating that the model has high accuracy in simulating deep ground temperature. The ME for shallow soil (≤0.20 m) is greater than 0, indicating that the model overestimated the T_{soil} to varying degrees, which was mainly caused by the overestimation of the ground temperature during winter season (Fig. 3). During the completely thawed period, the model underestimated the T_{soil} over the entire soil profile. This could be because the SHAW is only a one-dimensional coupled water flow and heat transport model, which only considers the vertical transmission of water and heat without considering lateral groundwater flow and the accompanying advective heat transport which could significantly affect the thermal-moisture regime of the active layer (Frampton et al. 2013; Rowland et al. 2011; Sjoberg et al. 2016). The SHAW model simply assumes the soil thermal conductivity and heat capacity as weighted values of various components in the soil (unfrozen water, ice, and soil particles), which may lead to a deviation in the calculation of thermal conductivity and heat capacity under extremely dry conditions in winter (Zhang et al. 2011). In addition, surface soil drying caused the surface albedo in winter to be generally higher than that in summer. The calculation error of the ground albedo caused by the deviation of the moisture simulation (Fig. 4) may also be one of the reasons for the overestimation of winter ground

temperature (Fig. 3). Generally, the simulation results are acceptable when 0.6≤NSE≤0.8 and the simulation accuracy of the model is considered to be excellent when NSE>0.8 (Chang et al. 2015). In this study, the NSE of T_{soil} simulation at different depths is greater than 0.88, which means that the simulation results are very reliable. Thus, according to the analysis of the model performance measures of the T_{soil} over the

entire soil profile, we can deduce that the developed SHAW model can accurately simulate the dynamic process of T_{soil}.

3.2 Soil moisture

Soil moisture in the active layer could affect evaportranspiration, sensible and latent flux, and soil
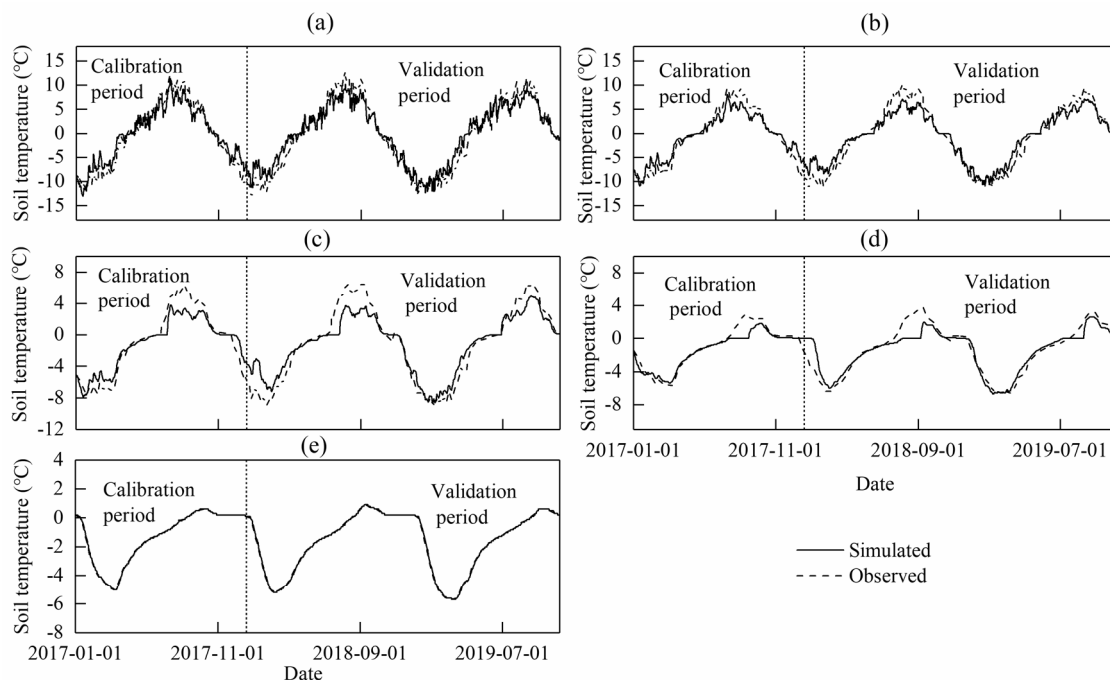

Fig. 3 Comparison of simulated and measured daily average soil temperature (T_{soil}) at (a) 0.05 m, (b) 0.20 m, (c) 0.50 m, (d) 1.00 m, (e) 1.60 m.
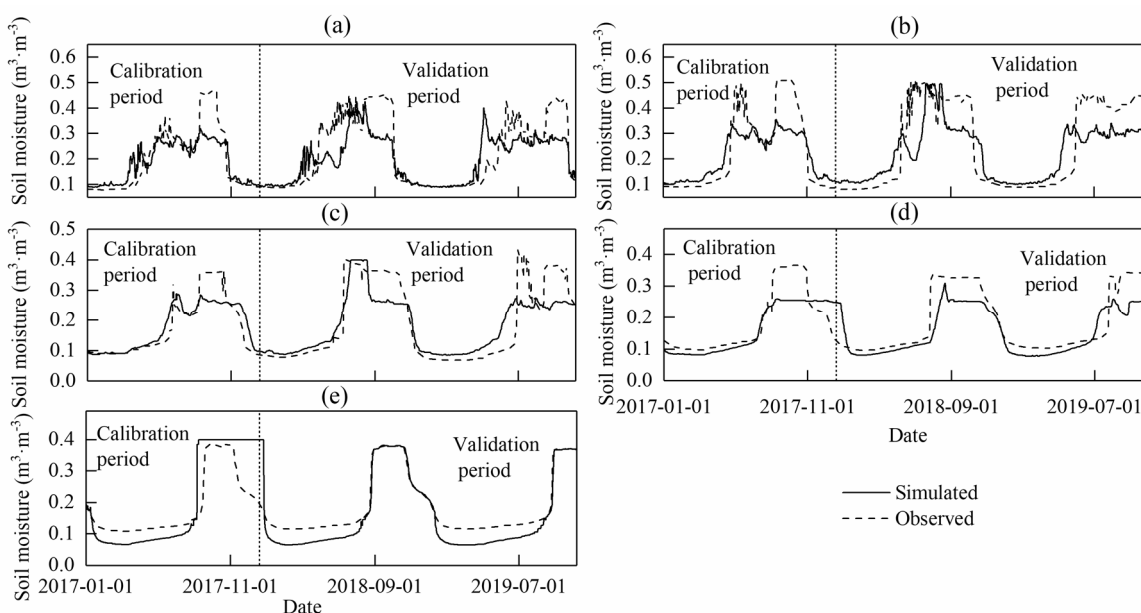

Fig. 4 Comparison of simulated and measured daily average soil water content at (a) 0.05 m, (b) 0.20 m, (c) 0.50 m, (d) 1.00 m, (e) 1.60 m.

Table 5 Model performance measures for soil moisture

Depth (m)	Calibration period (2017/1/1-12/31)			Validation period (2018/1/1-2019/10/31)		
	RMSE (m³·m⁻³)	ME (m³·m⁻³)	NSE	RMSE (m³·m⁻³)	ME (m³·m⁻³)	NSE
0.05	0.066	-0.011	0.719	0.090	-0.027	0.570
0.20	0.087	-0.017	0.689	0.105	-0.025	0.604
0.50	0.045	0.001	0.800	0.066	-0.008	0.746
1.00	0.056	-0.021	0.681	0.057	-0.030	0.662
1.60	0.090	0.020	0.200	0.043	-0.026	0.799

Notes: RMSE, ME, and NSE denote root mean square error, mean error, and Nash–Sutcliffe efficiency coefficient, respectively.

temperature, which are important issues in the study of land surface processes in permafrost regions (Zhao et al. 2008). Fig. 4 shows the dynamic changes of the measured and simulated volumetric soil unfrozen water content, and Table 5 summarizes the model performance measures for soil water content at different depths. According to our observations, the RMSE value varied in the range of 0.043–0.105, and t he NSE value varied in the range of 0.570–0.799 over the entire soil profile, and the accuracy of the M_{soil} simulation increased with the soil depth, which is similar to that of soil temperature simulation. The ME was less than zero over the entire soil profile, indicating that the developed SHAW model underestimated the M_{soil}, especially in the completely thawed period. One reason could be the SHAW model's low sensitivity to precipitation (Guo and Yang 2010), resulting in a small amount of simulated infiltration water. The other reason could be related to the propagation of the frozen fringe, the model overestimated the downward water migration, resulting in the lower M_{soil} at shallow depths [0.05–1.0 m, Fig. 4 (a)-(d)] and higher M_{soil} at the deeper depth [1.6 m, Fig. 4(e)]. The model overestimated the soil water content in the depth range of 0.05–0.50 m during winter [Fig. 4 (a)-(c)]. Previous studies have shown that this kind of overestimation of the M_{soil} during winter was due to simulation errors of the timing and rate of snow-deposition and ablation (Link et al. 2004; Zhang et al. 2011). The simulated soil moisture thaw-rise time was earlier than the actual observations over the entire soil profile (Fig. 4). This may be related to the overestimation of soil accumulated temperature which is mainly caused by the overestimation of the T_{soil} in winter (Fig. 3). Nevertheless, the developed SHAW model still captures the trend of soil moisture dynamics well. Generally, the accuracy of soil moisture simulation is not as good as that of T_{soil} simulation, which may be caused by many factors: (1) the soil thermal and hydraulic parameters, which are automatically calculated by the SHAW model, have a lot of

uncertainty; (2) the vegetation parameters, along with vegetation transpiration and the distribution of roots, significantly affect the soil water migration; and (3) the complex interactions between the surface ecosystems include the effects of the soil organic matter layer and thermal conductivity, along with their coupling effects on soil moisture dynamics (Sitch et al. 2003).

4 Results

4.1 Seasonal variation in surface energy fluxes

The simulated net radiation (R_n) showed the characteristics of high value in summer and autumn and low value in spring and winter (Fig. 5), and the annual mean values of R_n were found to be 104.4 ± 2.7, 103.3 ± 2.7, 100.3 ± 2.7, 98.5 ± 2.6, 96.6 ± 2.6, 86.4 ± 2.5, and 73.7 ± 2.3 W·m⁻² (Table 6) when RLC was +100%, +70%, +30%, 0%, -30%, -70%, and -100%, respectively. There was a significant difference ($P<0.05$) in the R_n under different RLCs in the growing-season, non-growing season, and for the whole year. The ground heat flux (G_0) varied from -21.8 to +23.4 W·m⁻² (15-day moving average), followed approximately the same trend of R_n during the whole year, and reached its maximum value in July when the solar altitude was the highest (You et al. 2017). The annual mean values of G_0 were found to be 0.8 ± 0.9, 1.0 ± 0.9, 1.2 ± 1.0, 1.6 ± 1.0, 1.6 ± 1.0, 1.7 ± 1.0, and 2.9 ± 1.0 W·m⁻² (Table 6) when RLC was +100 %, +70 %, +30 %, 0 %, -30 %, -70 %, and -100 %, respectively. This implies that the smaller the LAI, the more likely it is that the energy will be consumed to increase the soil temperature, resulting in a higher ground heat flux, which is consistent with the study of Wang et al. (2009) on the FHS.

During the growing season, with the arrival of the monsoon rains and sprouting plants, most energy was consumed in the latent heat (*LE*) with a mean value of 75.6 ± 2.9, 74.8 ± 2.7, 70.5 ± 2.4, 68.0 ± 2.4, 66.4 ±

2.3, 60.0 ± 2.1, and 54.5 ± 1.5 W·m^{-2} (Table 6) when the RLC was +100%, +70%, +30%, 0%, -30%, -70%, and -100%, respectively. The LE increased rapidly and reache   d its maximum in late July due to the relatively higher LAI and R_n (Fig. 5). The continuously decreasing land–atmosphere temperature difference [Fig. 6(a)] led to the reduction of energy consumed in the sensible heat (H/R_n), with a mean value of 0.38 ± 0.02, 0.38 ± 0.02, 0.39 ± 0.01, 0.40 ± 0.01, 0.40 ±

0.01, 0.41 ± 0.01 and 0.36 ± 0.01 (Table 6) when the RLC was +100%, +70%, +30%, 0%, -30%, -70%, and -100%, respectively, despite the fact that R_n maintained a relative higher value. During the non-growing season (with foliar senescence and decreasing precipitation), the LE decreased rapidly, and the H dominated the energy partitioning with a mean value of 78.6 ± 1.7, 76.6 ± 1.6, 73.5 ± 1.5, 71.7 ± 1.5, 71.2 ± 1.5, 60.3 ± 1.2, and 46.5 ± 0.9 W·m^{-2} (Table
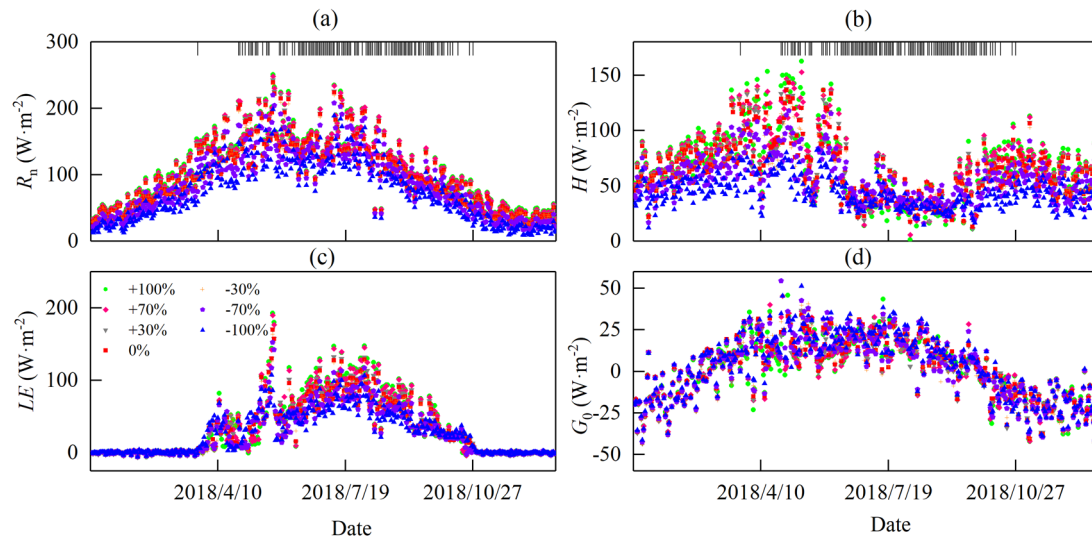

Fig. 5 Annual variations (left panels) in daily integrated (a) net radiation (R_n), (b) sensible heat (H), (c) latent heat (LE), and (d) ground heat flux (G_0) under different ratio of LAI changing (RLC), bars at the top represent rain events.

Table 6 Energy balance components (mean ± standard error determined from daily averages) under different ratio of LAI changing (RLC) during different periods from January 2018 to December 2018

Period	RLC item	Different RLC						
		+100%	+70%	+30%	0%	-30 %	-70 %	-100 %
Growing-season (May-September)	R_n (W·m^{-2})	143.2±3.2	142.5±3.1	138.6±3.1	137±3.1	134.3±3.0	125.3±2.8	111.3±2.5
	H (W·m^{-2})	54.0±2.9	54.2±2.7	54.2±2.4	54.4±2.4	53.9±2.2	49.9±1.7	39.1±1.1
	LE (W·m^{-2})	75.6±2.9	74.8±2.7	70.5±2.4	68.0±2.4	66.4±2.3	60.0±2.1	54.5±1.5
	G_0 (W·m^{-2})	13.6±0.8	13.5±0.9	13.9±0.8	14.6±0.8	14.0±0.9	15.4±0.8	17.3±0.8
	H/R_n	0.38±0.02	0.38±0.02	0.39±0.01	0.40±0.01	0.40±0.01	0.41±0.01	0.36±0.01
	LE/R_n	0.54±0.02	0.53±0.02	0.52±0.01	0.50±0.01	0.50±0.01	0.48±0.01	0.49±0.01
	G_0/R_n	0.09±0.01	0.09±0.01	0.09±0.01	0.10±0.01	0.09±0.01	0.11±0.01	0.14±0.01
Non-growing-season (October-April)	R_n (W·m^{-2})	76.4±2.7	74.9±2.7	72.6±2.7	70.7±2.7	69.4±2.6	58.4±2.4	46.5±2.2
	H (W·m^{-2})	78.6±1.7	76.6±1.6	73.5±1.5	71.7±1.5	71.2±1.5	60.3±1.2	46.5±0.9
	LE (W·m^{-2})	6.2±0.9	6.3±0.9	7.1±0.9	6.9±0.9	6.9±0.9	6.3±0.8	7.5±0.9
	G_0 (W·m^{-2})	-8.4±1.1	-8.0±1.2	-8.0±1.2	-7.9±1.2	-7.6±1.2	-8.1±1.2	-7.5±1.2
	H/R_n	1.17±0.02	1.17±0.02	1.17±0.03	1.18±0.03	1.2±0.03	1.28±0.04	1.42±0.06
	LE/R_n	0.05±0.01	0.06±0.01	0.07±0.01	0.07±0.01	0.07±0.01	0.07±0.01	0.10±0.01
	G_0/R_n	-0.22±0.02	-0.22±0.02	-0.24±0.02	-0.25±0.02	-0.27±0.02	-0.35±0.03	-0.52±0.05
Whole year	R_n (W·m^{-2})	104.4±2.7	103.3±2.7	100.3±2.7	98.5±2.6	96.6±2.6	86.4±2.5	73.7±2.3
	H (W·m^{-2})	68.3±1.7	67.2±1.6	65.4±1.4	64.4±1.4	63.9±1.3	55.9±1.0	43.4±0.7
	LE (W·m^{-2})	35.3±2.2	35.0±2.2	33.7±2.0	32.5±1.9	31.8±1.9	28.8±1.7	27.2±1.5
	G_0 (W·m^{-2})	0.8±0.9	1±0.9	1.2±1.0	1.6±1.0	1.6±1.0	1.7±1.0	2.9±1.0
	H/R_n	0.84±0.03	0.84±0.03	0.85±0.03	0.85±0.03	0.87±0.03	0.91±0.03	0.97±0.04
	LE/R_n	0.26±0.01	0.26±0.01	0.26±0.01	0.25±0.01	0.25±0.01	0.24±0.01	0.26±0.01
	G_0/R_n	-0.09±0.01	-0.09±0.01	-0.1±0.02	-0.1±0.02	-0.12±0.02	-0.15±0.02	-0.24±0.03

Notes: R_n, H, LE, and G_0 denote net radiation, sensible heat, latent heat, and ground heat flux, respectively.

6) when the RLC was +100%, +70%, +30%, 0%, -30%, -70%, and -100%, respectively. Both the *LE* and *H* increased with the *LAI* during the three periods (growing season, non-growing season, and the whole year).

4.2 Variations of evapotranspiration response to changes in leaf area index

Fig. 7 shows the variations of total evapotranspiration (E_{total}), vegetation transpiration (E_{trans}), soil evaporation (E_{soil}), and M_{soil} at 0.2 m of depth ($\theta_{0.2}$) under different RLCs, where E_{soil} is calculated by calculating the difference between E_{total} and E_{trans}. During the growing season, the E_{total} showed an increasing trend when the RLC varied from -100% to +100%, with a change by as much as 30%. However, the E_{total} changed irregularly when the LAI changed from -100% to +100% during the non-growing season. Additionally, from the scale of the

entire year, the E_{total} still shows an increase with decreasing LAI. When the RLC increased from -100% to 0%, the change ratio of the E_{trans} in the growing season, non-growing season, and for the whole year were as high as 100%, which was significantly greater than that (15%, 59% and 15% respectively) when the RLC increased from 0% to +100%, indicating a polynomial function relationship between E_{trans} and the LAI (Table 7).

Unlike E_{trans} and E_{total}, there is a negative correlation between E_{soil} and LAI, which is consistent with the study of Gu et al. (2008) on the northern QTP. However, E_{soil} in the growing season and over the whole year significantly increased only when the RLC decreased from -30% to -100%, with a variation of 15% and 14%, respectively. Both E_{trans} and E_{soil} show a significantly larger range of change when the RLC changed from -100% to 0%, indicating that, in the study area, evapotranspiration was more sensitive to vegetation change at a lower LAI level.
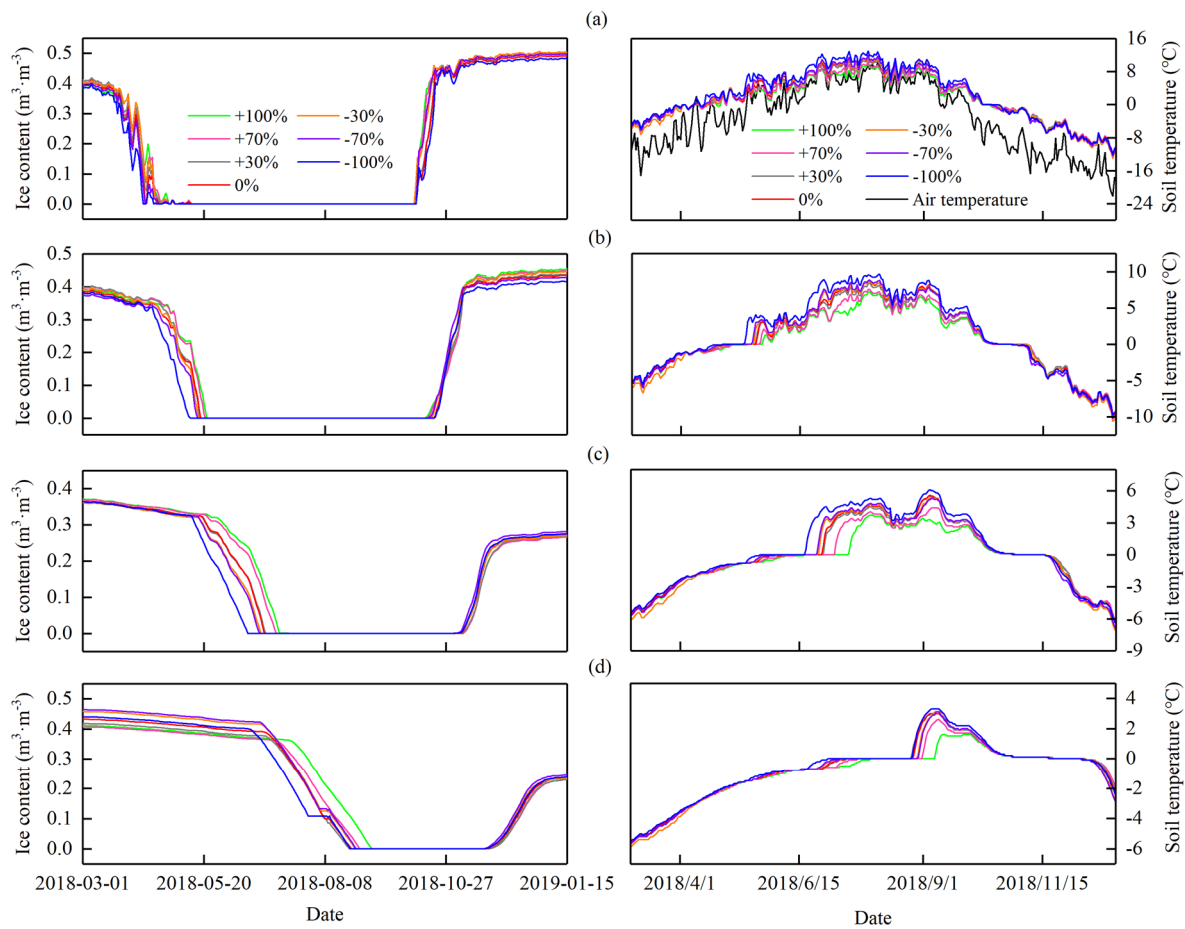

Fig. 6 Variations of soil ice content and soil temperature (T_{soil}) at (a) 0.05 m (with air temperature), (b) 0.2 m, (c) 0.5 m, (d) 1.0 m during thawing (left panels) and freezing (right panels) process under different ratio of LAI changing (RLC).
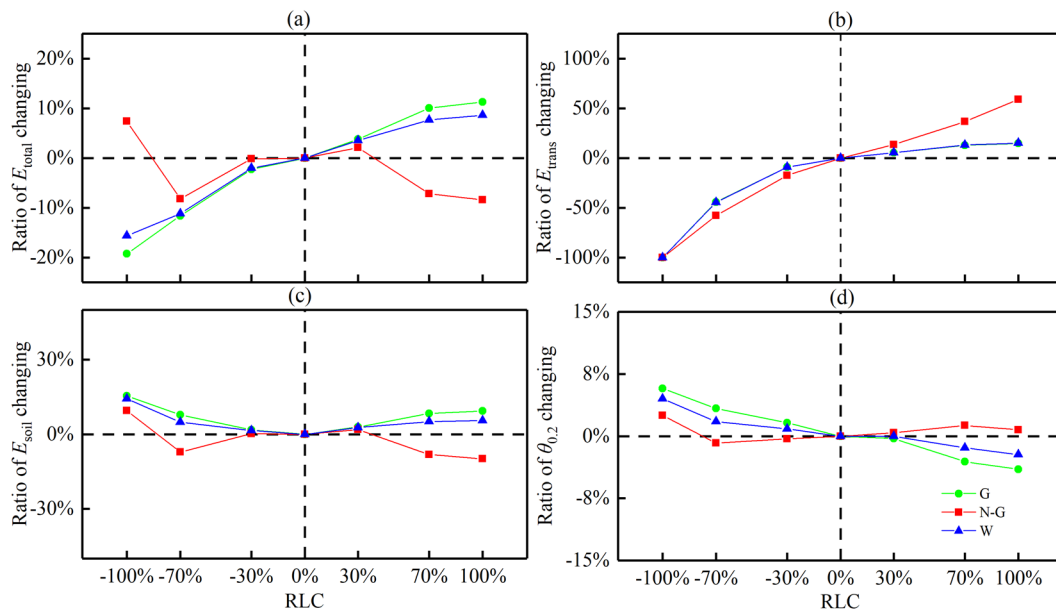
Fig. 7 Variation of (a) total evapotranspiration (E_{total}), (b) transpiration (E_{trans}), (c) soil evaporation (E_{soil}) and (d) soil moisture (M_{soil}) at 0.2 m ($\theta_{0.2}$) versus the ratio of LAI changing (RLC), N-G, G, and W denote the non-growing season, growing season, and whole year, respectively.

Table 7 Functional relationship between transpiration and ratio of LAI changing (RLC)

Period	Function	The coefficient of determination (R²)
Growing season	$y = -0.4360x^2 + 0.5029x + 0.0239$	0.97
Non-growing season	$y = -0.2059x^2 + 0.7409x - 0.0023$	0.99
Year	$y = -0.4339x^2 + 0.5052x + 0.0236$	0.97

Table 8 Characteristics of soil temperature (T_{soil}) indexes in the thawing ang freezing periods for different ratio of LAI changing (RLC) from January 2018 to December 2018

Depth (m)	+100%	+70%	+30%	0%	-30%	-70%	-100%	+100%	+70%	+30%	0%	-30%	-70%	-100%
	T_{ao} (mm-dd)							ΔT_{max} (°C)						
0.05	04-27	04-21	04-19	04-18	04-18	04-17	04-10	10.2	10.6	11.6	12	12	12	13
0.2	05-13	05-04	05-03	05-03	05-03	05-02	04-27	7.2	7.6	8.4	8.7	8.8	8.8	9.7
0.5	06-18	06-13	06-04	06-04	06-01	05-31	05-21	3.7	4.4	5.5	5.6	5.4	5.3	6.1
1.0	07-30	07-22	07-15	07-13	07-12	07-10	07-03	1.6	2.6	3	3	3.1	3.1	3.3
Depth (m)	+100%	+70%	+30%	0%	-30%	-70%	-100%	+100%	+70%	+30%	0%	-30%	-70%	-100%
	T_{bo} (mm-dd)							ΔT_{min} (°C)						
0.05	10-09	10-10	10-15	10-15	10-09	10-09	10-14	-12	-12	-12.3	-12.2	-13	-12.4	-11.9
0.2	11-06	11-06	10-30	10-29	10-30	10-28	10-27	-9.6	-9.6	-9.9	-9.8	-10.6	-10.2	-9.7
0.5	11-18	11-18	11-18	11-18	11-18	11-17	11-17	-6.2	-6.1	-6.4	-6.5	-7.1	-6.9	-6.4
1.0	12-13	12-13	12-13	12-12	12-11	12-10	12-11	-2.1	-2	-2.3	-2.4	-2.9	-2.9	-2.5

Notes: T_{ao} represents the first day when the soil temperature was greater than 0°C for 7 consecutive days; T_{bo} represents the first day when the soil temperature was less than 0°C for 7 consecutive days; ΔT_{max} represents the difference between summer ground temperature peak value and initial thawing temperature (0°C); ΔT_{min} represents the difference between the initial freezing temperature (0°C) and the minimum ground temperature at completely frozen period.

4.3 Variations of soil temperature of the active layer response to changes in leaf area index

Several indexes were selected to quantify the response of soil temperature to the change in plant canopy in the freezing-thawing processes (Table 8), following the studies conducted by Wang et al. (2012).

During the thawing process, the T_{ao} at 0.05 m of depth gradually advanced from 4/27 to 4/10 when the RLC changed from +100% to -100%. For the deep soil layer (1.0 m); the T_{ao} advanced from 7/30 to 7/3 when the RLC changed from +100% to -100%, indicating that the difference in the T_{ao} under different RLCs increased with increasing soil depth. However, the amplitude of the soil temperature during the thawing process (ΔT_{max})

at 0.05 m increased from 10.2°C to 13.0°C (ΔT=2.8°C) when the RLC changed from +100% to -100%. For the deep soil layer (1.0 m), the ΔT_{max} increased from 1.6°C to 3.3°C (ΔT=1.7°C when RLC changed from +100% to -100%. The difference in ΔT_{max} gradually decreased with increasing soil depth (Table 8). In contrast, during the freezing process, there are no significant differences in the T_{bo} under different RLCs, and the soil temperature freeze-fall amplitude (ΔT_{min}) under different RLCs, indicating that changes in the plant canopy mainly affect the thermal dynamics of the active layer during the thawing period, which is consistent with previous studies on the QTP (Wang et al. 2012; You et al. 2017).

5 Discussion

5.1 Effects of plant canopy on surface energy partitioning

5.1.1 Surface albedo and net radiation

Surface albedo, which is mainly affected by the type of surface cover, soil roughness, soil color, soil moisture, and solar height angle (Xiao et al. 2010; Yao et al. 2013), is one of the most important biophysical factors affecting the surface energy budget, along with the local and global climates (Halim et al. 2019). There is a negative correlation between the surface albedo and the soil water content and LAI since more efficient solar absorption of green plants (Baldocchi et al. 2004; Li et al. 2006). In our study, the simulation results showed an increasing trend of the R_n with increasing LAI (Table 6), especially in the growing season, where the R_n increased by 5% when the RLC increased by +100%, whereas it decreased by 19% when the RLC decreased to -100% (bare land). This is consistent with a previous study in the FHS area (Wang et al. 2009), despite the high simulated water content of the topsoil under a low LAI level considered in our study site (details in Section 5.2). This is particularly observed in the growing season because the soil moisture has a negligible influence on the surface albedo compared with the changes in the wetness of the plant leaves and the leaf angle relative to the sun when the leaves completely shade the soil (You et al. 2017).

5.1.2 Turbulent fluxes

The response of R_n to the changes in the LAI could affect the energy partitioning into the H and LE (Zhang et al. 2019). In our study, there is a positive correlation between H and LAI, despite the simulated decreasing difference between the ground and air temperatures with the increasing LAI, which is contrary to previous studies on the QTP (You et al. 2017; Zhang et al. 2019). One possible reason could be that the SHAW model is sensitive to the changes in the plant canopy and overestimated the increase in the R_n with the increase in the LAI, and the annual average H/R_n show an increase with decreasing LAI (Table 6), indicating that more energy was consumed in H. This shows that there is a positive feedback cycle between climate warming and vegetation degradation. Otherwise, at our study's site, there is a positive correlation between the H and the plant canopy cover under the low LAI level.

5.1.3 Ground heat flux

Previous studies suggested that the lower thermal conductivity of the canopy and root turf could restrain heat absorption in summer and dissipation in winter due to the abundant porosity and organic matter content of the soil (You et al. 2014). The simulated G_o decreased 7% when the RLC increased by +100%, whereas it increased 19% when the RLC decreased to -100% in the growing season (Table 6), indicating that vegetation functions like a "quilt", which reduces the heat transfer from the atmosphere to the active layer in the warming period; this is consistent with previous studies on the QTP (Gu et al. 2015; Gu et al. 2005; Luo et al. 2018a; Wang et al. 2009; You et al. 2017; Zhou et al. 2008). It is important to note that there is no significant difference between the RLCs in the non-growing season. For the whole year, the simulated G_o decreased by 49% when the RLC increased by +100%, whereas it increased by 85% when the RLC decreased to -100%. In other words, a better vegetation condition could protect the underlying permafrost and mitigate its potential degradation by affecting energy partitioning.

5.2 Effects of plant canopy on moisture dynamics of active layer

5.2.1 Effects of plant canopy on surface and shallow soil moisture

Kurc and Small (2004) reported that, for semi-arid grassland, the correlation between soil moisture

and evapotranspiration in the root zone of vegetation is stronger than that at any other depth. During the thawing process, a rapid increase in $\theta_{0.2}$ of the active layer resulted in a dramatic increase in evapotranspiration, and the *LE* increased rapidly and reached its maximum value when the topsoil was completely thawed in late July (Fig. 8). It should be noted that $\theta_{0.2}$ remained unchanged at 0.5 m³·m⁻³ from July 10 to August 10 when the RLC was <0. This is because the saturated volumetric moisture content of 0.2 m was set at 0.5, which means that the $\theta_{0.2}$ increases to more than 0.5 m³·m⁻³ when the RLC <0; the shallow soil moisture increased with decreasing LAI. During the freezing process, the *LE* decreased rapidly, with a decrease of $\theta_{0.2}$, and remained at a low level after the whole active layer was completely frozen (mid-November; Fig. 8). The $\theta_{0.2}$ and *LE* showed consistent variation characteristics during the freezing and thawing processes. Wang et al. (2003) reported that the degradation of the alpine meadow significantly reduced the soil water retention and made the soil dry. However, our results show that, in the growing season, $\theta_{0.2}$ decreased by 4% when the LAI increased by 100%, which may be due to the increasing vegetation interception. Meanwhile, the E_{trans} increased by 15%, which indicates that there is a negative feedback relationship between the soil moisture and the vegetation transpiration in the region. With the climate gradually changing warm and wet on the QTP (Zhang et al. 2018), the increase in the E_{total} may lead to an increase in soil water loss during the evapotranspiration process, and the decrease of soil water, in turn, restrains the above process subsequently. In addition, the influence of vegetation on the evapotranspiration process is not only related to its cover but also closely related to the location of grassland landform and vegetation types (Wang et al. 2003), which should be taken into account to fully understand the effect of vegetation change on evapotranspiration.

5.2.2 Effects of plant canopy on soil water phase change

The phase change of soil water within the active layer could affect the timing and amplitude of supra-permafrost groundwater, which will have a great influence on the water cycles in cold regions eventually (Gao et al. 2018). The difference in vegetation cover, soil water potential, and soil texture can lead to a different amount of phase change water during the freezing-thawing processes (Zhou et al. 2008).
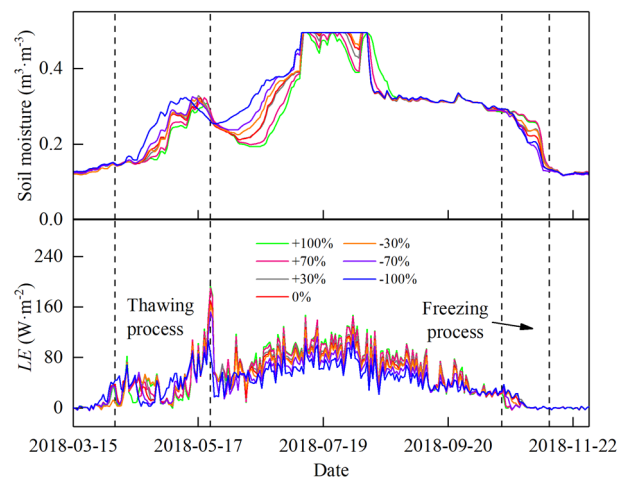

Fig. 8 Variation of soil moisture (M_{soil}) at 0.2 m ($\theta_{0.2}$, upper panel) and latent heat flux (LE, 15-day moving averages, lower panel) under different ratio of LAI changing (RLC).

However, in this study, the amounts of phase change water under different RLCs are almost identical (Fig. 6). Generally, the changes in vegetation cover, structure, and type are always accompanied by the changes in soil texture, bulk density, and organic matter contents (Wang et al. 2012), which have a great influence on soil infiltration, heat absorption and dissipation (Wang et al. 2007). None of these were considered in our study, except for the LAI, which may explain the "consistency" in the amount of phase change under different RLCs. During the thawing process, the initial thawing time of soil ice gradually advanced with decreasing LAI, and the thawing rate (the slope of the thawing curve) was also increased with the decrease of LAI (Fig. 6), which is mainly related to the small thermal conductivity of soil under high LAI conditions (Wang et al. 2012). In conclusion, we can infer that the continuous degradation of vegetation could advance the soil thawing time and increase the thawing rate and amount of thawing ice (Zhou et al. 2008), which may cause the early arrival of the flood period and increase the runoff, eventually, threatening the safety of life and property. During the freezing process, there was no significant difference in the phase change of the soil water under different RLCs, which is consistent with the response of soil temperature to the changes in the canopy. We will explain this in detail in the next section.

5.3 Effects of plant canopy on thermal dynamics of active layer

Previous studies have shown that dense

vegetation and peat deposits can retard the warming of the ground (Luo et al. 2018a; Luo et al. 2018b; Wang et al. 2009; You et al. 2017). Our study shows that, during the thawing process, the T_{soil} at each depth decreased with increasing LAI. During the freezing process, the T_{soil} appears to increase with increasing LAI after the temperature falls below 0°C (Fig.7). However, the differences in the T_{soil} during this period were small compared with those during the thawing process, which is consistent with previous studies on the FHS area (Wang et al. 2012; Zhou et al. 2008). The mechanism of T_{soil} (also the soil water) response to the changes in the canopy can be explained through the surface energy balance. During the growing season, G_o is negatively correlated with LAI, and G_o gradually increases from 13.6 ± 0.8 to 17.3 ± 0.8 when the RLC changed from +100% to -100%. More heat was transferred to the active layer to promote the increase of the soil temperature, while there was no significant difference in the G_o under different RLCs during the non-growing season. In addition, the increased thermal conductivity caused by the frozen meadow decreased its own insulation effect (Porada et al. 2016), which may explain why the vegetation affected the T_{soil} more significantly in the thawing process than in the freezing process.

The study by Wang et al. (2012) in FHS suggested that alpine meadows having higher vegetation cover had lower heat conductivities, and the T_{soil} decreased with increasing vegetation cover during the completely thawed period, which is consistent with our study. In addition, we observed the latent heat effect, which refers to an effect that maintains the soil temperature near 0°C over extended periods of freezing or thawing. In this study, for example, the duration of the T_{soil} at 0.2 m remained at about 0°C gradually decreased from 20 days to 13 days when the RLC changed from +100% to -100% during the thawing process, indicating that the latent heat effect became gradually significant with increasing LAI (Fig. 6), which is consistent with the study of Luo et al. (2018a) in the SAYR. Under the combined influence of climate change and human activities, the serious degradation of vegetation in the QTP has resulted in a continuous increase in the active layer thickness, and the permafrost in some areas has gradually transformed into seasonally frozen ground, which adversely affects the water resources and ecological environment (Kurylyk et al. 2016; Qin et al. 2017b). Therefore, we suggest that the implementation of an enhanced protected eco-environment,

particularly for surface vegetation is conducive to maintaining the thermal stability of the underlying permafrost, especially for thermally unstable permafrost having ground temperature greater than -0.5°C (Ran et al. 2018).

6 Conclusion

We investigated the characteristics of water-heat exchange between the land-atmosphere systems and the thermal-moisture dynamics of the active layer, and further explored the influence of plant canopy change on the above processes by using the SHAW model. The results suggest that: (1) the surface energy budget in the study area has obvious seasonal variation characteristics, and the R_n, LE, and H are all positively correlated with the LAI. However, there is a negative correlation between the G_o and LAI, reflecting the protective effect of vegetation on the permafrost; (2) there is a negative feedback between shallow soil moisture and vegetation through changing evapotranspiration, and in the study area, soil evaporation and canopy transpiration were more sensitive to vegetation change at a lower LAI level; (3) due to the varying response of G_o to the changes in the LAI during the freezing-thawing processes, the T_{soil} is negatively correlated with the LAI in the thawing period, while in the freezing process it is the opposite; (4) the negative correlation of the thawing time and rate of soil ice with the LAI may affect the timing and magnitude of the supra-permafrost groundwater.

This study explores the effects of plant canopy changes on the above processes by changing the LAI. Actually, vegetation changes, including the changes in vegetation cover, structure, and type, are always accompanied by changes in soil texture, bulk density, and organic matter content, which have significant effects on the energy balance, water cycles, and soil hydrothermal properties. Future research should consider the above factors to fully understand the effects of vegetation change on the hydrothermal processes of the alpine ecosystems in permafrost regions. Nevertheless, this study is also conducive to understanding the impacts of plant canopy changes on the water-heat exchange of alpine ecosystems comprehensively under climate change.

References

Baldocchi D, Xu L, Kiang N (2004) How plant functional-type, weather, seasonal drought, and soil physical properties alter water and energy fluxes of an oak-grass savanna and an annual grassland. Agric For Meteorol 123(1-2): 13-39. https://doi.org/10.1016/j.agrformet.2003.11.006

Chang J, Wang GX, Gao Y, et al. (2014) The influence of seasonal snow on soil thermal and water dynamics under different vegetation covers in a permafrost region. J Mt Sci 11(3): 727-745. https://doi.org/10.1007/s11629-013-2893-0

Chang J, Wang GX, Guo, LM (2019) Simulation of soil thermal dynamics using an artificial neural network model for a permafrost alpine meadow on the Qinghai-Tibetan plateau. Permafrost Periglac 30(3): 195-207. https://doi.org/10.1002/ppp.2003

Chang J, Wang GX, Mao TX (2015) Simulation and prediction of suprapermafrost groundwater level variation in response to climate change using a neural network model. J Hydrol 529: 1211-1220. http://dx.doi.org/10.1016/j.jhydrol.2015.09.038

Chen RS, Lv SH, Kang ES, et al. (2006) A Distributed Water-Heat Coupled (DWHC) model for mountainous watershed of an inland river basin (I): model structure and equations. Adv Earth Sci (08): 806-818 (In Chinese).

Chen SP, Chen JQ, Lin GH, et al. (2009) Energy balance and partition in Inner Mongolia steppe ecosystems with different land use types. Agric For Meteorol 149(11): 1800-1809. https://doi.org/10.1016/j.agrformet.2009.06.009

Christensen TR, Johansson T, Åkerman HJ, et al. (2004) Thawing sub-arctic permafrost: Effects on vegetation and methane emissions. Geophys Res Lett 31(4): L04501. https://doi.org/10.1029/2003GL018680

Fang Y (2013) Managing the Three-Rivers headwater region, China: from ecological engineering to social engineering. Ambio 42(5): 566-576. https://doi.org/10.1007/s13280-012-0366-2

Flerchinger GN, Saxton KE (1989) Simultaneous heat and water model of a freezing snow-residue-soil system I. Theory and Development. Trans ASAE 32(2): 565-571. https://doi.org/10.13031/2013.31040

Frampton A, Painter SL, Destouni G (2013) Permafrost degradation and subsurface-flow changes caused by surface warming trends. Hydrogeol J 21(1): 271-280. https://doi.org/10.1007/s10040-012-0938-z

Gao B, Yang DW, Qin Y, et al. (2018) Change in frozen soils and its effect on regional hydrology, upper Heihe basin, northeastern Qinghai-Tibetan Plateau. Cryosphere 12(2): 657-673. https://doi.org/10.5194/tc-12-657-2018

Gu LL, Yao JM, Hu ZY, et al. (2015) Comparison of the surface energy budget between regions of seasonally frozen ground and permafrost on the Tibetan Plateau. Atmos Res 153: 553-564. https://doi.org/10.1016/j.atmosres.2014.10.012

Gu S, Tang YH, Cui XY, et al. (2008) Characterizing evapotranspiration over a meadow ecosystem on the Qinghai-Tibetan Plateau. J Geophys Res Atmos 113(D8). https://doi.org/10.1029/2007JD009173

Gu S, Tang YH, Cui XY, et al. (2005) Energy exchange between the atmosphere and a meadow ecosystem on the Qinghai–Tibetan Plateau. Agric For Meteorol 129(3): 175-185. https://doi.org/10.1016/j.agrformet.2004.12.002

Guglielmin M, Evans CJE, Cannone N (2008) Active layer thermal regime under different vegetation conditions in permafrost areas. A case study at Signy Island (Maritime Antarctica). Geoderma 144(1): 73-85. https://doi.org/10.1016/j.geoderma.2007.10.010

Guo DL, Yang MX (2010) Simulation of soil temperature and moisture in seasonally frozen ground of central Tibetan Plateau by SHAW model. Plateau Meteor 29(06): 1369-1377 (In Chinese).

Halim MA, Chen HYH, Thomas SC (2019) Stand age and species composition effects on surface albedo in a mixedwood boreal forest. Biogeosciences 16(22): 4357-4375. https://doi.org/10.5194/bg-16-4357-2019

Han BH, Zhou BR, Yan YQ, et al. (2019) Analysis of vegetation coverage change and its driving factors over Tibetan Plateau from 2000 to 2018. Acta Agrestia Sin 27(06): 1651-1658 (In Chinese). https://doi.org/10.11733/j.issn.1007-0435.2019.06.023

Jorgenson MT, Racine CH, Walters JC, et al. (2001) Permafrost degradation and ecological changes associated with a warming climate in Central Alaska. Clim Change 48(4): 551-579. https://doi.org/10.1023/A:1005667424292

Karl TR, Trenberth KE (2003) Modern global climate change. Science 302(5651): 1719-1723. https://doi.org/10.1126/science.1090228

Kurc SA, Small EE (2004) Dynamics of evapotranspiration in semiarid grassland and shrubland ecosystems during the summer monsoon season, central New Mexico. Water Resour Res 40(9): W09305. https://doi.org/10.1029/2004WR003068

Kurylyk BL, Hayashi M, Quinton WL, et al. (2016) Influence of vertical and lateral heat transfer on permafrost thaw, peatland landscape transition, and groundwater flow. Water Resour Res 52(2): 1286-1305. https://doi.org/10.1002/2015WR018057

Langford JE, Schincariol RA, Nagare RM, et al. (2020) Transient and Transition Factors in Modeling Permafrost Thaw and Groundwater Flow. Groundwater 58(2): 258-268. https://doi.org/10.1111/gwat.12903

Li DS, Wen Z, Cheng QG, et al. (2019) Thermal dynamics of the permafrost active layer under increased precipitation at the Qinghai-Tibet Plateau. J Mt Sci 16(2): 309-322. https://doi.org/10.1007/s11629-018-5153-5

Li SG, Eugster W, Asanuma J, et al. (2006) Energy partitioning and its biophysical controls above a grazing steppe in central Mongolia. Agric For Meteorol 137(1-2): 89-106. https://doi.org/10.1016/j.agrformet.2006.03.010

Link TE, Flerchinger GN, Unsworth M, et al. (2004) Simulation of water and energy fluxes in an old-growth seasonal temperate rain forest using the simultaneous heat and water (SHAW) model. J Hydrometeorol 5(3): 443-457. https://doi.org/10.1175/1525-7541(2004)005%3C0443:SOWAEF%3E2.0.CO;2

Luo DL, Jin HJ, He RX, et al. (2018a) Characteristics of water-heat exchanges and inconsistent surface temperature changes at an elevational permafrost site on the Qinghai-Tibet Plateau. J Geophys Res Atmos 123(18): 10404-10422. https://doi.org/10.1029/2018JD028298

Luo DL, Jin HJ, Marchenko SS, et al. (2018b) Difference between near-surface air, land surface and ground surface temperatures and their influences on the frozen ground on the Qinghai-Tibet Plateau. Geoderma 312: 74-85. https://doi.org/10.1016/j.geoderma.2017.09.037

Magnin F, Josnin JY, Ravanel L, et al. (2017) Modelling rock wall permafrost degradation in the Mont Blanc massif from the LIA to the end of the 21st century. Cryosphere 11(4): 1813-1834. https://doi.org/10.5194/tc-11-1813-2017

O'Donnell JA, Harden JW, McGuire AD, et al. (2011) Exploring the sensitivity of soil carbon dynamics to climate change, fire disturbance and permafrost thaw in a black spruce ecosystem. Biogeosciences 8(5): 1367-1382. https://doi.org/10.5194/bg-8-1367-2011

Porada P, Ekici A, Beer C (2016) Effects of bryophyte and lichen cover on permafrost soil temperature at large scale. Cryosphere 10(5): 2291-2315. https://doi.org/10.5194/tc-10-2291-2016

Qian J, Wang GX, Ding YJ, et al. (2006) The land ecological evolutional patterns in the source areas of the Yangtze and Yellow Rivers in the past 15 years, China. Environ Monit Assess 116(1-3): 137-156.
https://doi.org/10.1007/s10661-006-7232-2

Qin YH, Wu TH, Zhao L, et al. (2017a) Numerical modeling of the active layer thickness and permafrost thermal state across Qinghai - Tibetan Plateau. J Geophys Res Atmos 122(21): 11,604-11,620.
https://doi.org/10.1002/2017JD026858

Qin Y, Yang DW, Gao B, et al. (2017b) Impacts of climate warming on the frozen ground and eco-hydrology in the Yellow River source region, China. Sci Total Environ 605-606: 830.
https://doi.org/10.1016/j.scitotenv.2017.06.188

Ran YH, Li X, Cheng GD (2018) Climate warming over the past half century has led to thermal degradation of permafrost on the Qinghai-Tibet Plateau. Cryosphere 12(2): 595-608.
https://doi.org/10.5194/tc-12-595-2018

Rasmussen LH, Zhang WX, Hollesen J, et al. (2018) Modelling present and future permafrost thermal regimes in Northeast Greenland. Cold Reg Sci Technol 146: 199-213.
https://doi.org/10.1016/j.coldregions.2017.10.011

Rowland JC, Travis BJ, Wilson CJ (2011) The role of advective heat transport in talik development beneath lakes and ponds in discontinuous permafrost. Geophys Res Lett 38(17): L17504.
https://doi.org/10.1029/2011GL048497

Shur YL, Jorgenson MT (2007) Patterns of permafrost formation and degradation in relation to climate and ecosystems. Permafrost Periglac 18(1): 7-19.
https://doi.org/10.1002/ppp.582

Sitch S, Smith B, Prentice IC, et al. (2003) Evaluation of ecosystem dynamics, plant geography and terrestrial carbon cycling in the LPJ dynamic global vegetation model. Glob Change Biol 9(2): 161-185.
https://doi.org/10.1046/j.1365-2486.2003.00569.x

Sjoberg Y, Coon E, Sannel ABK, et al. (2016) Thermal effects of groundwater flow through subarctic fens: A case study based on field observations and numerical modeling. Water Resour Res 52(3): 1591-1606.
https://doi.org/10.1002/2015WR017571

Wang GX, Hu HC, Liu GS, et al. (2009) Impacts of changes in vegetation cover on soil water heat coupling in an alpine meadow of the Qinghai-Tibet Plateau, China. Hydrol Earth Syst Sci 13(3): 327-341.
https://doi.org/10.5194/hess-13-327-2009

Wang GX, Liu GS, Li CJ, et al. (2012) The variability of soil thermal and hydrological dynamics with vegetation cover in a permafrost region. Agric For Meteorol 162-163(3): 44-57.
https://doi.org/10.1016/j.agrformet.2012.04.006

Wang GX, Shen YP, Qian J, et al. (2003) Study on the influence of vegetation change on soil moisture cycle in alpine meadow. J Glaciol Geocryol (06): 653-659 (In Chinese).
https://doi.org/10.3969/j.issn.1000-0240.2003.06.010

Wang GX, Wang YB, Li YS, et al. (2007) Influences of alpine ecosystem responses to climatic change on soil properties on the Qinghai–Tibet Plateau, China. Catena 70(3): 506-514.
https://doi.org/10.1016/j.catena.2007.01.001

Wang YH, Yang HB, Gao B, et al. (2018) Frozen ground degradation may reduce future runoff in the headwaters of an inland river on the northeastern Tibetan Plateau. J Hydrol 564: 1153-1164.
https://doi.org/10.1016/j.jhydrol.2018.07.078

Wen Z, Niu FJ, Yu QH, et al. (2014) The role of rainfall in the thermal-moisture dynamics of the active layer at Beiluhe of Qinghai-Tibetan plateau. Environ Earth Sci 71(3): 1195-1204.
https://doi.org/10.1007/s12665-013-2523-8

Xiao Y, Zhao L, Li R, et al. (2010) The characteristics of surface albedo in permafrost regions of northern Tibetan Plateau. J Glaciol Geocryol 32(03): 480-488 (In Chinese).

Yao JM, Gu LL, Zhao L, et al. (2013) Comparatively observational study of the surface albedo between the permafrost region and the seasonally frozen soil region. Acta Meteorol Sin 71(01): 176-184 (In Chinese with English abstract).
https://doi.org/10.11676/qxxb2013.015

Yi SH, McGuire AD, Harden J, et al. (2009) Interactions between soil thermal and hydrological dynamics in the response of Alaska ecosystems to fire disturbance. J Geophys Res Biogeosci 114(G2): 92-103.
https://doi.org/10.1029/2008JG000841

Yin GA, Niu FJ, Lin ZJ, et al. (2016) Performance comparison of permafrost models in Wudaoliang Basin, Qinghai-Tibet Plateau, China. J Mt Sci 13(7): 1162-1173.
https://doi.org/10.1007/s11629-015-3745-x

You QG, Xue X, Peng F, et al. (2017) Surface water and heat exchange comparison between alpine meadow and bare land in a permafrost region of the Tibetan Plateau. Agric For Meteorol 232: 48-65.
https://doi.org/10.1016/j.agrformet.2016.08.004

You QG, Xue X, Peng F, et al. (2014) Comparison of ecosystem characteristics between degraded and intact alpine meadow in the Qinghai-Tibetan Plateau, China. Ecol Eng 71: 133-143.
https://doi.org/10.1016/j.ecoleng.2014.07.022

Zhang ML, Wen Z, Dong JH, et al. (2018) Coupled water-vapor-heat transport in shallow unsaturated zone of active layer in permafrost regions. Rock Soil Mech 39(02): 561-570 (In Chinese).
https://doi.org/10.16285/j.rsm.2017.1128

Zhang PC, Shao GF, Zhao G, et al. (2000) Ecology - China's forest policy for the 21st century. Science 288(5474): 2135-2136.
https://doi.org/10.1126/science.288.5474.2135

Zhang W, Wang GX, Zhou J, et al. (2012) Simulating the water-heat processes in permafrost regions in the Tibetan Plateau based on CoupModel. J Glaciol Geocryol 34(05): 1099-1109 (In Chinese).

Zhang X, Liu XQ, Zhang LF, et al. (2019) Comparison of energy partitioning between artificial pasture and degraded meadow in three-river source region on the Qinghai-Tibetan Plateau: A case study. Agric For Meteorol 271: 251-263.
https://doi.org/10.1016/j.agrformet.2019.02.046

Zhang YL, Cheng GD, Li X, et al. (2017) Influences of frozen ground and climate change on hydrological processes in an alpine watershed: a case study in the upstream area of the Hei'he River, Northwest China. Permafrost Periglac 28(2): 420-432.
https://doi.org/10.1002/ppp.1928

Zhang YS, Ohata T, Zhou J, et al. (2011) Modelling plant canopy effects on annual variability of evapotranspiration and heat fluxes for a semi-arid grassland on the southern periphery of the Eurasian cryosphere in Mongolia. Hydrol Process 25(8): 1201-1211.
https://doi.org/10.1002/hyp.7885

Zhang Y, Wang GX, Wang YB (2010) Response of biomass spatial pattern of alpine vegetation to climate change in permafrost region of the Qinghai-Tibet Plateau, China. J Mt Sci 7(4): 301-314.
https://doi.org/10.1007/s11629-010-2011-5

Zhao L, Li R, Ding YJ (2008) Simulation on the soil water-thermal characteristics of the active layer in Tanggula range. J Glaciol Geocryol 30(06): 930-937 (In Chinese).

Zhong L, Ma YM, Xue YK, et al. (2019) Climate change trends and impacts on vegetation greening over the Tibetan Plateau. J Geophys Res Atmos 124(14): 7540-7552.
https://doi.org/10.1029/2019JD030481

Zhou J, Kinzelbach W, Cheng GD, et al. (2013) Monitoring and modeling the influence of snow pack and organic soil on a permafrost active layer, Qinghai-Tibetan Plateau of China. Cold Reg Sci Technol (90-91): 38-52.
https://doi.org/10.1016/j.coldregions.2013.03.003

Zhou J, Wang GX, Li X, et al. (2008) Energy-water balance of meadow ecosystem in cold frozen soil areas. J Glaciol Geocryol 30(03): 398-407 (In Chinese).

Zou DF, Zhao L, Sheng Y, et al. (2017) A new map of permafrost distribution on the Tibetan Plateau. Cryosphere 11(6): 2527-2542.
https://doi.org/10.5194/tc-11-2527-2017